Intellectual Disability and Behavioral Deficits Linked to CYFIP1 Missense Variants Disrupting Actin Polymerization

Intellectual Disability and Behavioral Deficits Linked to *CYFIP1* Missense Variants Disrupting Actin Polymerization

Vittoria Mariano[1,2], Alexandros K. Kanellopoulos[1], Carlotta Ricci[3], Daniele Di Marino[4], Sarah C. Borrie[2], Sebastian Dupraz[5], Frank Bradke[5], Tilmann Achsel[1], Eric Legius[2], Sylvie Odent[6,7], Pierre Billuart[8], Thierry Bienvenu[8] and Claudia Bagni[1,3]

[1]Department of Fundamental Neurosciences, University of Lausanne, 1005 Lausanne, Switzerland.
[2]Department of Human Genetics, KU Leuven, 3000 Leuven, Belgium.
[3]Department of Biomedicine and Prevention, University of Rome Tor Vergata, 00133 Rome, Italy.
[4]Department of Life and Environmental Sciences, New York-Marche Structural Biology Center (NY-MaSBiC), Polytechnic University of Marche, 60131 Ancona, Italy.
[5]Axonal Growth and Regeneration Group, German Center for Neurodegenerative Diseases (DZNE), Venusberg-Campus 1, Building 99, 53127 Bonn, Germany.
[6]Service de Génétique Clinique, Centre Labellisé pour les Anomalies du Développement Ouest, Centre Hospitalier Universitaire de Rennes, 35203 Rennes, France.
[7]Institut de Génétique et Développement de Rennes, CNRS, UMR 6290, Université de Rennes, ERN ITHACA, France.
[8]Institut de Psychiatrie et de Neurosciences de Paris (IPNP), Institut National de la Santé et de la Recherche Médicale (INSERM) U1266, Université de Paris Cité (UPC), Paris 75014, France.

***Corresponding author:** Claudia Bagni, Ph.D.
Email: Claudia.Bagni@unil.ch; Claudia.Bagni@uniroma2.it;
Tel (1): +41-216925120; Tel (2): +39-0672596063

Keywords: CYFIP1, Autism Spectrum Disorder, Actin remodeling, Drosophila, Social deficits, Motor impairment.

Short running title: *CYFIP1* SNVs Affect Actin Polymerization and Behavior

Abstract

Background: 15q11.2 Deletions and duplications have been linked to autism spectrum disorder (ASD), schizophrenia, and intellectual disability (ID). Recent evidence suggests that dysfunctional *Cytoplasmic FMR1 Interacting Protein 1 (CYFIP1)* contributes to the clinical phenotypes observed in individuals with 15q11.2 deletion/duplication syndrome. *CYFIP1* plays crucial roles in neuronal development and brain connectivity, promoting actin polymerization and regulating local protein synthesis. However, the impact of single nucleotide variants in *CYFIP1* to neurodevelopmental disorders is limited.

Methods: Here, we report a family with two probands exhibiting ID, ASD, spastic tetraparesis, and brain morphology defects carrying biallelic missense point mutations in the *CYFIP1* gene. We used skin fibroblasts from one of the proband, parents, and typically developing individuals to investigate the effect of the variants on the functionality of *CYFIP1.* In addition, we generated *Drosophila* knock-in mutants to address the effect of the variants *in vivo* and gain insight into the molecular mechanism underlying the clinical phenotype.

Results: Our study revealed that the two missense variants are in protein domains responsible for maintaining the interaction within the wave regulatory complex (WRC). Molecular and cellular analyses in skin fibroblasts from one proband showed deficits in actin polymerization. The fly model for these mutations exhibited abnormal brain morphology and F-actin loss and recapitulated the core behavioral symptoms, such as deficits in social interaction and motor coordination.

Conclusions: Our findings suggest that the two *CYFIP1* variants contribute to the clinical phenotype observed in the proband that reflects deficits in actin-mediated brain development processes.

Introduction

The 15q11.2 (BP1-BP2) has emerged as a susceptibility locus for neuropsychiatric disorders, including intellectual disabilities and neurobehavioral disturbances (1-6). Copy number variants (CNV) in the 15q11.2 region have been identified in patients with autism spectrum disorders (ASD), schizophrenia (SCZ), neurodevelopmental delay, intellectual disability (ID) and epilepsy (1, 5, 7-17). Although, four genes are present within the human BP1-BP2 region (*TUBGCP5, CYFIP1, NIPA2*, and *NIPA1*), increasing evidence points to the relevance of *Cytoplasmic FMR1 Interacting Protein 1* (*CYFIP1*). Due to its crucial role in synaptic development and functionality (18, 19), neuronal connectivity (19, 20), brain wiring (21, 22) and GABAergic signaling (23, 24), dysregulation of *CYFIP1* has been suggested to contribute to the clinical phenotype observed in patients with 15q11.2 variations. *CYFIP1* CNVs have been associated with ASDs, SCZ, epilepsy, and cognitive deficits (2, 8, 10, 11, 15, 17, 25-33). Single nucleotide variants (SNV) in coding regions affecting the protein sequence have been reported in ASD cases (34-36) and in an individual with congenital heart disease and learning disability (37). In addition, SNVs in the noncoding regions of the *CYFIP1* gene have been detected in large-scale whole genome sequencing (WGS) studies in cohorts affected by ASD (38-41). Finally, GWAS-ATLAS reveals *CYFIP1* association with neurological and metabolic disorders (42). However, the precise role of CYFIP1 in those clinically relevant cases remains elusive.

CYFIP1 plays a role in neurodevelopment by linking FMRP-dependent local protein synthesis with actin cytoskeleton remodeling through Rac1 small GTPase signaling (18, 43). When bound to Rac1, CYFIP1 is part of the Wave Regulatory Complex (WRC), containing WAVE1/2/3, ABI1/2, NCKAP1 and HPSC300 (44-46), which regulates the actin nucleation activity of the Arp2/3 complex. Under basal conditions, CYFIP1 inhibits the Arp2/3 complex, while upon binding of Rac1-GTP, CYFIP1 conformational change in the WRC allows activation of the Arp2/3 complex and actin polymerization (45-53). Fine-tuned actin cytoskeleton dynamics plays a crucial role in

neurodevelopmental processes such as dendritic spine morphology (54), axonal guidance and branching (55), and synapse functionality (56, 57).

This study aimed to understand how SNVs in *CYFIP1* could contribute to neurodevelopmental deficits. We report a family case with two probands carrying biallelic missense variants in the *CYFIP1* gene, one variant inherited from each parent. Individuals are affected by severe ID and ASD, together with epileptic encephalopathy, spastic tetraparesis, and microcephaly. Parents do not show the clinical phenotype reported for the probands. Using available skin fibroblasts from one of the probands, parents and typical developing individuals, and *Drosophila* CRISPR knock-in (KI) models for the two missense variants, we investigated the impact of these SNVs on the functionality of CYFIP1 and their contribution to the clinical phenotype of the proband.

Methods and Materials

Ethics statements. Human skin fibroblasts from Proband 1 and their parents were received from clinical collaborators and coauthors of this study. All procedures performed in this study were in accordance with the ethical standards of the French Institute Cochin research committee and with the Declaration of Helsinki of 1964 and its subsequent amendments. Written informed consent to the molecular diagnosis of genetic diseases was obtained from parents.

Human fibroblast cell lines. Fibroblasts from healthy volunteers (typically developing individuals (TDI) were obtained from: 1) purchased from Coriell Institute Cell Repositories (Camden, NJ); 2) UZ/KU Leuven Biobank (Dr. Hilde Van Esch, Belgium) and previously described (58, 59) (n = 4, age range 22-33 years and n = 3 age 42-57). Human fibroblasts from father (I-1), mother (I-2) and proband 1 (II-2) were obtained from the Institut Cochin, Université de Paris (France). See Supplemental Information for culture conditions.

Live imaging and analysis of actin cytoskeleton remodeling. Cells on glass bottom plates (MatTek) were transfected with CMV-Lifeact-EGFP (60) using Lipofectamine 2000 transfection reagent (Invitrogen, Thermo Fisher Scientific) in Opti-MEM (Gibco, Thermo Fisher Scientific). After 6 h, the medium was replaced and 24 h cells were imaged. Time-lapse imaging was performed for 2 min/cell, on a Nikon A1R Eclipse Ti for fast and high-resolution acquisition. Argon laser at 5% and 60x objective (UPlanSApo, NA 1.2, water immersion) were used. A chamber around the microscope kept the sample at a constant temperature of 37 °C, CO_2 level and humidity. Kymographs were generated from pixel-wide lines drawn orthogonally to the cell edge in regions where lamellar protrusions of fibroblasts were actively protruding, using FIJI (61).

Fly stocks and genetics. Flies were maintained on standard cornmeal fly food at 25 ° C, 60 % humidity, in a 12-h light/dark cycle. Wild type cantonized w^{1118} (23, 62) flies were used as control. All transgenic lines tested were initially backcrossed into the w^{1118} background. Because the two variants are present in a boy, male flies 5-7 days after eclosion were used for all experiments. Behavioral experiments were performed between ZT1-ZT4 (Zeitgeber Time). Detailed information on CRISPR/Cas9 generation of the *Drosophila* Cyfip-KI mutants, immunofluorescence, mushroom body morphometric measurement and behavioral experiments are provided in Supplemental Information.

Statistics. Analyses were performed using GraphPad Prism software (v.9). The Shapiro-Wilk test for normal distribution of the data was used. Statistical tests are listed in the respective figure legends. *p*-values < 0.05 were considered significant. The results are represented as mean ± standard error of the mean (S.E.M.).

See Supplemental Information for description of the following methods: exome sequencing, description and in silico analysis of the sequence variants, variant validation, structural variant modeling, RNA isolation and qPCR, western blotting, surface sensing of translation (SUnSET) assay, immunofluorescence, and immunoprecipitation of the CYFIP1 complex.

Results

Exome sequencing and genetic analyses reveal potentially pathogenic missense variants in *CYFIP1*

We identified a non-consanguineous family with two individuals (II-2 and II-3) affected by a severe neurodevelopmental disorder (Figure 1A). Both individuals show developmental delay, microcephaly (with head circumference (HC) below 2 standard deviations), inability to walk without assistance, and absence of speech, consistent with a severe form of intellectual disability (ID). ID was classified in both probands as severe or profound (according to DSM-5 criteria (63)). The two probands exhibit autistic symptoms characterized by a “pseudo-Angelman” phenotype (paroxysmal laughter and happy demeanor) and severe motor deficits. Proband 1 shows hyperactivity and repetitive self-mutilating behavior (head-banging). Frequent generalized non-motor seizures with onset between 3-6 years of age have been detected in both probands. Brain FLAIR magnetic resonance imaging reported white matter hyperintensities in the thalamus with moderate ventriculomegaly in proband 1. Table 1 reports a detailed summary of the clinical characteristics of the two probands. Clinical evaluations report that neither of the parents (I-1 and I-2) has clinical phenotypes. The family also has one unaffected sibling (II-1).

We performed Whole Exome Sequencing (WES) analysis on proband 1 (II-2) and his parents (I-1 and I-2). In total 26’060 to 26’216 single nucleotide polymorphisms (SNPs) and 902 to 906 small deletions/insertions (1-10 bp) were identified across the exomes of this family. After testing for *de novo*, recessive and X-linked inheritance and filtering the variants for moderate/high pathogenicity score impact (PolyPhen-2, SIFT, CADD and REVEL scores), we identified 14 potential pathogenic genetic variants (Table 2). Pathogenic variants that were not detected in both probands and that were not involved in syndromic disorders that could explain the clinical phenotype were excluded. We narrowed the list down to two biallelic variants in the *Cytoplasmic FMRP interacting protein 1* (*CYFIP1)* gene, potentially involved in the neurodevelopmental disorder of the probands. The

variant p.(Ile476Val), inherited from the father (15/152142 alleles in gnomAD v.3.0) was reported tolerated, disease-causing, and “possibly damaging” by the pathogenicity prediction tools. The variant p.(Pro742Leu), inherited from the mother (6/152210 alleles) was predicted to be tolerated and benign by *in silico* analysis. Both missense variants were also detected in the second proband and were confirmed by direct Sanger sequencing. Genetic analysis showed that the probands were compound heterozygotes, while the parents and the sibling are heterozygotes for a single variant (Figure 1A-B). Considering these findings and the prominent roles of *CYFIP1* in neurodevelopment, we focused our attention on understanding the role of the two *CYFIP1* SNVs.

We utilized the available crystal structure of the human WRC (45, 64) to map the two CYFIP1 variants (Figure 1C-D). The p.(Ile476Val) variant is situated in the globular N-domain, in proximity to the RAC1 binding site A (Figure 1C)(45). The isoleucine residue is embedded within a complex set of secondary structural elements, specifically α-helices (Figure 1D, lower insets). Our hypothesis suggests that the substitution of valine for isoleucine at position 476 could potentially destabilize the structure of CYFIP1, due to the smaller size and lower hydrophobicity of valine compared to isoleucine, resulting in a decrease in hydrophobicity. This would lead to a subtle disruption in the contacts between the two secondary structural elements of the proteins and hinder interaction with the amino acids Leu605 and Phe608 (Figure 1D, lower insets). This is further supported by the protein stability analysis, which estimates a ΔΔG value of + 1.28 ± 0.036 kcal/mol for the Ile476Val variant.

The p.(Pro742Leu) variant is located in the central domain, that confers structural flexibility to CYFIP1 (Figure 1C), and contributes to the binding with the translation factor eIF4E and to the interactions with WAVE1 and NCKAP1 in the WRC (45, 47, 48, 51, 64-66). A butterfly-like motion has been associated with the ability of CYFIP1 to switch from the WAVE complex towards the eIF4E complex (43, 65), suggesting that the decrease in flexibility associated with the Pro742Leu mutation could affect this switching ability (Figure 1D, upper insets). This is consistent with the

protein stability analysis, which revealed that this variation has a slightly destabilizing effect on the 3D structure of CYFIP1 with a ΔΔG value of + 0.72 ± 0.023 kcal/mol (Figure 1D, upper insets). Importantly, both variants affect amino acid regions that are highly conserved between taxa, from humans to fruit flies (Figure 1E), underlying the relevance of these domains.

Bi-allelic *CYFIP1* variants underlie a complex disorder affecting actin remodeling

To determine the effect of the missense variants in *CYFIP1* at the functional level, we used the available skin fibroblasts from proband 1, the two parents and age-matched typical developing individuals (TDI). No defective levels of *CYFIP1* mRNA (Figure 2A) and protein levels (Figure 2B) were observed in proband 1, neither differences in expression for the other genes deleted in the BP1-BP2 deletion syndrome (*NIPA1, NIPA2,* and *TUBGCP5*), nor the Angelman syndrome-associated gene *UBE3A* (Figure S1A).

CYFIP1 coordinates cytoskeletal actin remodeling through interactions with the WRC (18, 20, 67) and protein synthesis through interactions with FMRP and eIF4E (18, 19, 33, 43, 68). Impairments in these molecular mechanisms are notably implicated in ASD pathogenesis (34, 68-74). We performed surface sensing of translation (SUnSET) (75) to measure relative protein synthesis rates in human fibroblasts (58). No differences in puromycin incorporation were observed between fibroblasts from the proband and/or parents and TDI individuals, suggesting that these variants do not affect overall protein synthesis levels (Figure S1B). In contrast, using phalloidin-TRITC immunofluorescence to detect filamentous (F) actin (Figure 3A), we found that fibroblasts from the proband 1 displayed a reduction in phalloidin intensity and therefore, F-actin levels (Figure 3B). In addition, an increase in the aspect ratio (AR: major axis/minor axis, Figure 3C) in the proband fibroblasts, indicated a subtle and yet significative change in cell morphology from a typical spindle-like to a more stellate-shaped cell phenotype (Figure 3D).

F-actin remodeling is crucial for lamellar protrusion and cell motility (76). We performed live imaging of actin lamellar protrusion dynamics in TDI and proband 1 fibroblasts after transfection with Lifeact-GFP (60) to allow visualization of F-actin dynamics (77). Kymograph analysis of the lamellar protrusions (Figure 3E) revealed a significant reduction in protrusion length, number, and velocity (Figure 3F-H) in proband 1 cells, confirming the actin polymerization defects observed in the presence of bi-allelic *CYFIP1* variants. Next, we investigated whether the two missense variants affect the interaction of CYFIP1 within the WRC. We coprecipitated the CYFIP1-WRC complex from TDI (Figure 3I-K, lane 1-3) and proband 1 (Figure 3I, lane 4-6) fibroblasts and assessed the levels of CYFIP1 interactors with known involvement in Arp2/3 activation and actin remodeling (44, 49, 50, 64, 78, 79). Notably, a significant reduction of CYFIP1 interaction with NCKAP1 and WAVE1 in the proband 1 compared to TDI fibroblasts was observed (Figure 3I-K). Collectively, these results suggest that the biallelic missense variants in the cells of proband 1 possibly impair the WRC functionality in actin polymerization due to the reduced CYFIP1 stability inside the complex leading to the deficits in cytoskeleton actin dynamics.

CYFIP **SNVs recapitulate human deficits in actin polymerization in** ***Drosophila***

We utilized the model organism *Drosophila melanogaster* to investigate the effects of bi-allelic *CYFIP1* missense variants on ID/ASD pathologies. Notably, *Drosophila* has been extensively used to model specific aspects of human pathologies (80-82). The *Drosophila* genome contains a single homolog (*Cyfip*) (83) of the two vertebrate genes, *CYFIP1* and *CYFIP2*, with high homology (DIOPT score 15/18, 65% amino acid identity and 80% similarity). Alignment of the human CYFIP1 and the *Drosophila* Cyfip protein sequences revealed that the SNVs-containing regions are conserved in the two organisms (Figure 4A), therefore, using the *scarless* CRISPR-Cas9 gene-editing approach (Figure 4B), we generated knock-in (KI) fly lines for the human

missense variants, the p.(Ile476Val), p.(Ile471Val) in the fly genome and the p.(Pro742Leu) variant, p.(Pro760Leu) in the fly genome.

While the *Cyfip* homozygous null mutants are lethal at the pupa stage (83). The homozygous KI animals (*Cyfip*^{I471V}/*Cyfip*^{I471V} and *Cyfip*^{P760L}/*Cyfip*^{P760L}) and the compound heterozygous genotype (*Cyfip*^{I471V}/*Cyfip*^{P760L}) were viable, fertile, and did not display visible morphological phenotypes. No differences in *Cyfip* mRNA levels were detected in mutant flies (Figure S2A), consistent with the previous observation in human skin fibroblasts (Figure 2A). Therefore, we asked if the actin polymerization deficits observed upon the presence of the two variants were recapitulated within the KI fly model system. We performed biochemical fractionation to measure the F- and globular (G) actin amounts in the control and *Cyfip* mutant heads. F-actin appeared to be significantly reduced compared to G-actin in *Cyfip*^{I471V}/*Cyfip*^{P760L} flies in comparison to control and parental lines, as shown by the reduced F-/G- actin ratio (Figure 4C). These results show that flies carrying both *Cyfip* variants, exhibit actin cytoskeleton deficits, like the molecular phenotypes observed in the human cells.

CYFIP **SNVs affect neuronal morphology in** ***Drosophila***

CYFIP1 has been shown to regulate dendrite morphogenesis and axonal growth, pathfinding, and branching (67, 84). To determine whether the missense *CYFIP1* variants affect neuronal morphology in the fly model, we analyzed the structure of a well-characterized subset of neurons called small lateral ventral neurons (s-LNvs). Their stereotyped axonal projection pattern (Figure 4D-E) allows studies of axonal arborization phenotypes (85, 86). Changes in s-LNvs axonal 3D arborization were analyzed in *Cyfip* mutant flies and control flies (Figure 4D-F), as previously described (87). 3D spread analysis of the dorsal s-LNvs termini (Figure 4G) showed a decreased in the spread of the arborizations in flies carrying the two missense variants, compared to control

flies and to flies heterozygous for the single missense variant. In addition, the axonal volume occupied by the dorsal axonal projections was reduced in the *Cyfip*$^{I471V/P760L}$ and *Cyfip*$^{P760L/+}$ mutants compared to the control flies (Figure 4H), indicating a morphological deficit. To further investigate the brain morphology in the different *Cyfip-KI* mutant flies, we conducted morphology analyses of the mushroom bodies (MB) and the ellipsoid body (EB), high brain structures involved in behaviors, from learning and memory, to social behavior and motor skills (88, 89) (Figure S2B-C). No gross morphological defects were observed in mutant flies, however, a detailed morphometric analysis (89) of the different structures revealed consistent subtle differences in neuroanatomical organization. We quantified the widths and lengths of α- and β-lobes and surface areas of the ellipsoid body (Figure S2D-F), uncovering significant differences in α- and β-lobe lengths between control and *Cyfip*^{I471V}/*Cyfip*^{P760L} flies (Figure S2D). In addition, the α-lobe length in heterozygous flies for the single and the double variants was significantly increased, while the β-lobe length was increased in *Cyfip*^{I471V}/*Cyfip*^{P760L} and in *Cyfip*$^{P760L/+}$ flies (Figure S2D). No changes in the α- and β-lobes width was observed (Figure S2E). Finally, an increase in the ellipsoid surface relative to the control was observed in heterozygous flies for the two single variants and in biallelic variant flies (Figure S2F). In summary, we showed that biallelic *Cyfip* missense variants in flies induces axonal lobe extension defects, suggesting that the biallelic presence of the *CYFIP1* variants negatively impacts the neuronal and brain morphology in flies.

CYFIP **SNVs showed ASD-like behaviors in** ***Drosophila***

CYFIP1 heterozygosity in animal models induced cognitive impairments (15), ASD- and SCZ-like behaviors (22, 62, 90) including social and motor deficits (21-23, 90, 91).

Male flies were tested for competition for food (aggression paradigm), a well-established social behavior assay (23) (Figure 5A). *Cyfip*$^{I471V/+}$, *Cyfip*$^{P760L/+}$ and *Cyfip*^{I471V}/*Cyfip*^{P760L} flies showed

fewer social events than controls, indicating that the Cyfip variants contribute to the aggression phenotype and their combination exacerbate this phenotype (Figure 5B and Video S1). Second, we assessed fly social group behavior using the Social Space Arena paradigm (Figure 5C). Analyzing the overall social space distribution between each fly, we observed that most control flies (> 40%) spend time at a close distance (< 0.5 cm). In contrast, *Cyfip-KI* mutants exhibit a different distribution in the arena (Figure 5D). Notably, *Cyfip*^{I471V}/*Cyfip*^{P760L}, *Cyfip*$^{I471V/+}$ and *Cyfip*$^{P760L/+}$ flies distribute in the arena at farther distance from each other compared to control flies. In addition, the social preference index as in (92, 93) revealed a decreased index for the Cyfip variants (Figure 5E). Overall, our analyses suggest that the *Cyfip* missense variants give susceptibility to social interaction defects strengthening the role of CYFIP in regulating social interactions (23).

Additionally, we assessed motor skills in the flies carrying the missense variants. We evaluated motor reflex as the ability to climb after sudden stimuli (namely, negative geotaxis behavior) (Figure 5F) (94). The number of flies above a 6 cm distance 9 seconds after the startle input was recorded (Figure 5G). The number of *Cyfip*^{I471V}/*Cyfip*^{P760L} flies above the target line compared to control and flies with the missense variant in heterozygosity was significantly reduced. No difference was observed between controls and *Cyfip*$^{I471V/+}$ and *Cyfip*$^{P760L/+}$ (Figure 5G and Video S2). The reduced climbing behavior of *Cyfip*^{I471V}/*Cyfip*^{P760L} flies might be related to deficits in motor reflexes or reflect a general locomotion deficit. To tease these apart, we assessed the total locomotion (activity paradigm) (Figure 5H-I). Activity analysis revealed a reduced number of total beam crossings in the bi-allelic mutants *Cyfip*^{I471V}/*Cyfip*^{P760L} compared to control, to *Cyfip*$^{I471V/+}$ and *Cyfip*$^{P760L/+}$ flies, reflecting reduction in locomotion in the presence of both missense variants (Figure 5I). These results confirm that the bi-allelic presence of the missense variants induces motor deficits, including motor reflex deficits and hypo-activity in *Drosophila*.

Discussion

Previous reports have identified SNVs in *CYFIP1* in individuals with neurodevelopmental disorders (NDD) or affected by ASD and learning disabilities (34-41), with no clinical evaluation or investigation of the pathogenicity. Here, we report a complete clinical, molecular, and functional characterization of two rare biallelic missense variants in the *CYFIP1* gene, predicted to be deleterious and pathogenic. The two probands are affected by severe ID, motor deficits, repetitive behavior, and social deficits. Notably, alterations in pathways regulated by CYFIP1 lead to cellular (*i.e.,* spine structure and neurotransmission) and molecular (*i.e.,* actin dynamics and protein synthesis) (18, 19, 23, 24, 33, 43, 68, 91, 95) defects possibly contributing to the severe phenotype. *CYFIP1* haploinsufficiency in animal models revealed deficits in brain connectivity abnormalities and ASD/SCZ- like behavioral phenotypes, *i.e.,* social interaction, repetitive behaviors, learning, and sensory-motor processing (15, 21-23, 90).

The two variants cluster with domains relevant for the CYFIP1 function. In *silico* structural modeling analysis revealed that the amino acid substitutions could impair the flexibility, the motions of the secondary structure, and the network of hydrophobic interactions, possibly affecting binding to eIF4E or to WRC (45, 47, 48, 51, 65, 96). Protein synthesis was not affected by the presence of the missense variants, while a general reduction of actin cytoskeleton dynamics and polymerization was observed. These findings are supported by the protein stability analysis and immunoprecipitation experiments, indicating that the identified SNVs destabilize the CYFIP1 structure inside the WRC, with the Pro742Leu and Ile476Val mutations acting inter- and intra-molecularly, respectively, and impairing the interaction between CYFIP1 and its binding partners, NCKAP1 and WAVE1. This disruption is likely to lead to WRC function defects that might explain the observed phenotypes in the actin cytoskeleton and lamellar behavior in Proband 1 fibroblasts. Notably, NCKAP1 and WAVE family protein, including WAVE1, are known to regulate the activity of Arp2/3 complex-mediated actin assembly (45, 50, 52, 64, 97-100),

necessary to promote cell shape, motility, and functionality. In line with our findings, F-actin polymerization is reduced upon disruption of the CYFIP1-NCKAP1 interaction in dendritic spines (18) and actin remodeling, migration and lamellipodia formation are impaired after NCKAP1 abrogation (49, 101). In addition, lamellipodia protrusion length deficits, reduced F-actin at leading edges and deficits in dorsal ruffles formation and actin elongation have been observed upon WAVE1 deletion (97, 102-104).

Dysregulation in actin polymerization causes neuronal and glial developmental abnormalities (105), leading to ASD and neurological disorder, including seizures (106-109). Fine-tuned cytoskeleton function regulates proper spine morphology, with spine abnormalities likely to confer susceptibility to epilepsy due to disruptions to the excitatory/inhibitory (E/I) balance of neuronal circuitries (110). E/I balance and GABAergic signaling dysregulations have been described in animal models for *CYFIP1* haploinsufficiency, from flies to mice (23, 24). Interestingly, epileptic encephalopathy, and intellectual disability have also been reported in patients with missense variants in the *CYFIP1*-homologous gene, *CYFIP2* (106, 111, 112). *Drosophila Cyfip* null mutant exhibit impaired axonal growth, guidance, and branching (20, 83). *CYFIP1* deficiency has been shown to reduce axonal growth (84) and to regulate axonal outgrowth (67). We observed that the *CYFIP*1 variants affect mushroom bodies and ellipsoid body morphology and s-LNvs neurons axonal branching in *Drosophila*. Interestingly, *Rho, Cdc42* and *Rac1* over-expression in these neurons in *Drosophila* induces axonal branch overgrowth (87), a phenotype opposite than the one observed in the *Cyfip-KI* bi-allelic mutants. We speculate that the reduced axonal projection and volume that we observed in flies harboring the bi-allelic missense variants might be related to deficits in actin polymerization. However, other mechanisms – such as guidance cues, neuronal activity, and neurotransmitter release (55, 113, 114), not depending on actin remodeling - might be involved in the observed cellular phenotype.

Social and motor coordination deficits are hallmarks of ASD and NDDs (115) and reported within the 15q11.2 deletion (7, 13). These phenotypes have also been described in animal models for *CYFIP1* haploinsufficiency with brain connectivity abnormalities and motor coordination deficits (21-23, 90). The observed behavioral deficits in social interaction and motor skills in flies harboring the *CYFIP*1 missense variants, suggest that the combination of both Cyfip I471V and Cyfip P760L contribute to the clinical phenotypes of the two probands. Furthermore, in the social domains, social deficits have also been observed in the presence of single missense variants in heterozygosity. Although mutants carrying the single or both missense mutations show a similar pattern for certain cellular and behavioral phenotypes, the variability in the data make us cautious to conclude on the specific contribution of each variant while the presence of both variants result in a clear more severe phenotype. Consistently, it was shown that the combination of rare and recessive biallelic mutations contribute to the pathogenicity of NDDs and ASD (116-120).

In conclusion, we reported a rare case of biallelic missense variants in the *CYFIP1* gene in two individuals with NDD. Using the fly model, we investigated their impact in the absence of the confounding effects of genetic background gaining insights on the pathogenicity underlying the relevance of *CYFIP1* in NDDs. Variants in the *CYFIP1* gene can represent susceptibility factors for variable cognitive, neurological, and psychiatric disorders and may result in severe NDDs such as those observed in the probands. Future work on KI mouse models and brain organoids will complement our study to further clarify the functional consequences of *CYFIP1* variants in mammalian brain development.

Acknowledgments: We thank the probands and the family for participating in this study. We thank Nicolas Lebrun for technical assistance, Patrick Nitschké and members of the Cochin Hospital Cell Bank and Bioinformatics platforms (Institut Imagine) for technical and bioinformatics assistance. The co-author Dr. Sylvie Odent is a member of the European Reference Network on Rare Congenital Malformations and Rare Intellectual Disability ERN-ITHACA. We thank Dr. Hilde Van Esch (UZ Leuven, Belgium) and UZ Biobank (Belgium) for generously providing one of the TDI fibroblast cell line. We thank the Developmental Hybridoma Studies Bank for antibodies, FlyCRISPR and Flybase for informations, Prof. Brian McCabe (EPFL) for sharing reagents, grateful to Arianna Ravera (DCSR, University of Lausanne) for the 3D reconstruction of the sLNv axonal projections. We thank the Bagni laboratory for inputs and discussion on this work and A. Crevoisier and J. Viguie for excellent administrative and technical support, Nuria Dominguez-Iturza for confocal imaging assistance, Giulia Cencelli for sharing samples, Adrian Lo for support with the custom R scripts and Marie Fagotto Kaufmann for helping with some of the initial experiments. We acknowledge Dr. Kris Dickson for comments and initial editing the the manuscript. C.B. was supported by Etat de Vaud, SNFS 310030-182651, NCCR Synapsy 51NF40-158776, Novartis Foundation for medical-biological research (Switzerland), ERANET-NEURON Joint Transnational Research Projects on Sensory Disorders 2020-088, PRIN 201789LFKB MIUR and Telethon GGP20137 (Italy), KULeuven Opening the Future, UCB Award, Queen Elizabeth Foundation (Belgium). VM is a recipient of Women in Science (WIS) Award 2022, A.K.K was supported by Autism Speaks Meixner Translational Postdoctoral Fellowship (No 9728), and Pierre Mercier Foundation (Switzerland). F.B. is supported by the DZNE, the International Foundation for Research in Paraplegia, Wings for Life, the Deutsche Forschungsgemeinschaft, ERANET AXON REPAIR, and ERANET RATER SCI. F.B. is a member of the excellence cluster ImmunoSensation2 (EXC2151–390873048). ChatGPT was used as a proofreader for the revised version.

Competing interests: The authors report no biomedical financial interests or potential conflicts of interest.

Figure Legends

Figure 1: Identifications of two missense variants in human *CYFIP1.*

(A) Pedigree chart showing segregation of rare pathogenic *CYFIP1* variants c.1426A > G; p.(Ile476Val) and c.2225C > T; p.(Pro742Leu) in the family. Unfilled shapes denote typically developing individuals (TDI), while filled shapes denote probands; squares are males; circles are females. (B) Electropherograms of Sanger sequencing of genomic DNA of exons 14 and 20 of the *CYFIP1* from the family members (I-1, I-2, II-2 and II-3). The variants are highlighted in yellow. For exon 20 the overlapping peaks have been detected as “N” (an ambiguous, or unknown base) from the automatic detection software and interpreted as “T”. (C) Schematic representation of the CYFIP1 protein (NP_001274739.1). The functional domains are color coded: in magenta and orange (Rac1-binding sites), green (WAVE1-VCA), blue (Abi2-HSPC300) and purple (eIF4E), Arf1 (grey) respectively (45, 46, 51, 53, 65, 66). The putative FMRP binding region is shown in light blue (18, 43, 121). In light yellow the putative NCKAP1 binding regions (45, 47, 52, 66). Asterisks indicate missense variants, in black, the previously identified in individuals with ASD and learning disabilities (34-37) and in red the new identified variants in this work. (D) Structure of the WAVE regulatory complex (WRC) indicating the sites of *CYFIP1* variants. CYFIP is shown in red. Amino acid residues affected by missense variants are enlarged in circles. Next to each substitution the ΔΔG value is reported. (E) Alignment of human CYFIP1 protein (NP_001274739.1) against the mouse (NP_001158133.1), zebrafish (NP_997924.1) and *Drosophila* (NP_650447.1) homologs showing the conservation of sequences where the missense mutations are located. The variants identified in the probands are marked in light blue.

Figure 2: Characterization of the *CYFIP1* missense variants.

(A) Quantification of *CYFIP1* mRNA levels by real-time qPCR in the affected individual (proband 1, p.[(Ile476Val)];[(Pro742Leu)]) compared to TDI (3 lines, 22-33 years old and 1 line, 50 years old) and parents (the father, p.[(Ile476Val)];[(=)]) and the mother p. [(=)]; [(Pro742Leu)]) fibroblasts. TDI n = 12, Proband 1 n = 3, Father n = 3, Mother n = 3, technical replicate. One-Way ANOVA, n.s. not significant. Data are represented as mean ± S.E.M. (B) Left, representative Western blot showing CYFIP1 in fibroblasts from the proband 1, parents and TDI (4 lines 22-33 years old and 2 lines 50-57 years old). Right, bar plots showing the quantification of CYFIP1 levels normalized over Vinculin, α-Tubulin, and total protein content. TDI n = 31, Proband 1 n = 6, Father n = 7, Mother n = 7, technical replicates. One-Way ANOVA. n.s. not significant. Data are represented as mean ± S.E.M.

Figure 3: Impact of human *CYFIP1* missense variants on actin polymerization.

(A) Representative images of primary fibroblasts from Proband 1, parental and TDI lines stained with phalloidin-TRITC to detect F-actin and DAPI for nuclei (Scale bar = 55 µm). Quantification TRITC fluorescent intensity (B) and aspect ratio (C-D) in the proband 1, parents and TDI (4 lines 22-33 years old and 3 lines 43-57 years old), fibroblasts. (C) Schematic representation of the Aspect Ratio parameter. Created with BioRender.com. Dots represent the quantification of a technical replicate performed on cells at different passage (TDI n = 26, Proband 1 = 5, Mother = 5, Father = 5, 50-60 cells for each line). One-Way ANOVA followed by Sidak's multiple comparison test; exact significant *p*-values are reported in the figure. Data are represented as mean ± S.E.M. (E) Representative kymographs at the level of the lamellar protrusions extracted from the fibroblasts from the Proband 1 and TDI (2 lines of 22 years). Quantification of length (F) number (G) and velocity (H) of lamellar protrusions. Dots represent kymographs from TDI (2 lines, n = 131 and Proband 1 n = 82, from 18-20 cells per genotype recorded and analyzed) (scale bar = 1 µm). (F and H) unpaired Student's t-test. (G) Mann Whitney test, exact significant *p*-values are reported in the figure. Data are represented as mean ± S.E.M. (I-J) Representative Western

blot showing the CYFIP1 immunoprecipitated complex from TDI (2 lines) and Proband 1 fibroblasts protein extracts (lanes 1-3 and 4-6, respectively, Input) and the detection of NCKAP1 (I) and WAVE1 (J). (K) Quantification of NCKAP1 and WAVE1 in the CYFIP1 immunoprecipitated complex. The protein levels were normalized to the immunoprecipitated CYFIP1 levels. Dots represent the quantification of a technical replicate performed on cells at different passages. NCKAP1 (TDI n = 16, Proband 1 n = 9), WAVE1 (TDI n = 8, Proband 1 n = 5). Multiple t-test corrected for multiple comparisons using Holm-Sidak method, exact significant *p*-values are reported in the figure. Data are represented as mean ± S.E.M.

Figure 4: Modelling the human *CYFIP1* missense variants in *Drosophila.*

(A) Alignment of the protein sequences of the human CYFIP1 with the fly CYFIP showing the similarity in the region affected by the missense variants. The variants identified in the probands are marked in light blue. (B) Generation of *Cyfip*^{I471V} and *Cyfip*^{P760L} alleles using the *scarless* genome editing approach. (C) Upper panel: representative Western blots for F-actin and G-actin levels from *Drosophila* whole brain. Lanes belongs to the same blot, n = 5-6 (pool of 20 fly heads) in control and *Cyfip* KI flies. Lower panel: Quantification of the F/G actin ratio normalized to control flies. One-way ANOVA followed by Sidak's multiple comparisons test, exact significant *p*-values are reported in the figure. Data are represented as mean ± S.E.M. (D-H) 3D structure analysis of the s-LNvs axonal arborization in control and *Cyfip* KI mutant flies. (D) Schematic representation of an hemibrain of *Drosophila* with highlighted the location and structure of the s-LNvs axonal dorsal projections. Left insets show a schematic magnification of the s-LNv dorsal projections and a max intensity confocal projection s-LNvs dorsal projections stained with PDF antibody. (E) Representative 3D reconstructions of the s-LNv dorsal projections showing the local z- and y axis. (F) Representative confocal max intensity projections of the s-LNv dorsal projections in control and *Cyfip* mutant flies (upper panels, scale bar = 10 µm) and their 3D reconstructions (lower panels) (z-axis in blue-to-red color scale), 1 pixel = 0.06 µm and z-step size = 1 µm (see

Supplemental Materials and Methods for details). (G - H) Quantification of the 3D spread (G) and the axonal 3D volume (H) covered by the axonal arborization. n = 24-29 axonal projections from 14-15 brains per genotype. One-way ANOVA followed by Sidak's multiple comparisons test: exact significant *p*-values are reported in the figure. Data are represented as mean ± S.E.M.

Figure 5: Effects of the human *CYFIP1* missense variants on *Drosophila* social and motor behaviors.

(A-B) Control and *Cyfip* mutant flies were analyzed for the total number of social interactions in a competition for food assay. (A) Schematic representation of the behavioral protocol and setup for the competition for food assay. (B) Quantification of the total number of social interaction events. n > 10 (pool of 8 male flies each, from 3-5 independent experiments). One-way ANOVA followed by Sidak's multiple comparisons test; exact significant *p*-values are reported in the figure. Data are represented as mean ± S.E.M. (C-E) Social space behavior. (C) Representative images of the social space arena in control and *Cyfip* mutant flies. Different distances among flies are depicted in circles: in red, a close distance (0-0.5 cm) and in blue (1.0 – 1.5 cm) (scale bar = 1 cm). (D) Distance to the closest flies indicated as percentage distribution of flies in the indicated ranges of distances, 0 - 0.5 cm, 0.5 - 1.0 cm, 1.0 -1.5 cm and > 1.5 cm bins. n > 8 arenas of 29-30 flies each per genotype. Kolmogorov–Smirnov test was assessed on the total distribution of the distances to the closest fly, exact significant *p*-values are reported in the figure. Data are represented as mean ± S.E.M. (E) Social preference (social space index) based on the distribution of flies over a 1 cm maximum distance. n > 8 arenas per genotype. One sample t- test compared to equal preference (0), exact significant p-values are reported in the figure. Data are represented as mean ± S.E.M. (F-G) Rapid Iterative Negative Geotaxis climbing assay (RING) in control and *Cyfip* KI mutants. (F) Schematic representation of the climbing assay (negative geotaxis) behavioral protocol. (G) Quantification of the number of flies (in percentage) that climbed the 6 cm distance in 9 seconds after sudden stimulus. n > 11 (groups of 17-20 flies each). One-way

ANOVA followed by Sidak's multiple comparisons test; exact significant *p*-values are reported in the figure. Data are represented as mean ± S.E.M. (H-I) Locomotor activity in control and *Cyfip* KI mutants measured with the *Drosophila* Activity Monitoring System (DAMs, Trikinetics). (H) Schematic representation of the experimental setup composed of an activity monitoring tube for individual fly activity recording. The monitoring tubes are in an incubator with control light dark cycle and automatically recorded. Created with BioRender.com. (I) Quantification of the total activity in control and *Cyfip* KI mutants. Activity (beam crossings) over 24 hr. n = 70-100 flies per genotype, from > 3 independent experiments. One-way ANOVA followed by Sidak's multiple comparisons test: exact significant *p*-values are reported in the figure. Data are represented as mean ± S.E.M.

References

1. Abdelmoity AT, LePichon JB, Nyp SS, Soden SE, Daniel CA, Yu S (2012): 15q11.2 proximal imbalances associated with a diverse array of neuropsychiatric disorders and mild dysmorphic features. *J Dev Behav Pediatr*. 33:570-576.
2. Burnside RD, Pasion R, Mikhail FM, Carroll AJ, Robin NH, Youngs EL, et al. (2011): Microdeletion/microduplication of proximal 15q11.2 between BP1 and BP2: a susceptibility region for neurological dysfunction including developmental and language delay. *Hum Genet*. 130:517-528.
3. Butler MG (2017): Clinical and genetic aspects of the 15q11.2 BP1-BP2 microdeletion disorder. *J Intellect Disabil Res*. 61:568-579.
4. Kirov G, Pocklington AJ, Holmans P, Ivanov D, Ikeda M, Ruderfer D, et al. (2012): De novo CNV analysis implicates specific abnormalities of postsynaptic signalling complexes in the pathogenesis of schizophrenia. *Mol Psychiatry*. 17:142-153.
5. Vanlerberghe C, Petit F, Malan V, Vincent-Delorme C, Bouquillon S, Boute O, et al. (2015): 15q11.2 microdeletion (BP1-BP2) and developmental delay, behaviour issues, epilepsy and congenital heart disease: a series of 52 patients. *Eur J Med Genet*. 58:140-147.
6. Chaste P, Sanders SJ, Mohan KN, Klei L, Song Y, Murtha MT, et al. (2014): Modest impact on risk for autism spectrum disorder of rare copy number variants at 15q11.2, specifically breakpoints 1 to 2. *Autism Res*. 7:355-362.
7. Cox DM, Butler MG (2015): The 15q11.2 BP1-BP2 microdeletion syndrome: a review. *Int J Mol Sci*. 16:4068-4082.
8. Zhao Q, Li T, Zhao X, Huang K, Wang T, Li Z, et al. (2013): Rare CNVs and tag SNPs at 15q11.2 are associated with schizophrenia in the Han Chinese population. *Schizophr Bull*. 39:712-719.
9. Stefansson H, Meyer-Lindenberg A, Steinberg S, Magnusdottir B, Morgen K, Arnarsdottir S, et al. (2014): CNVs conferring risk of autism or schizophrenia affect cognition in controls. *Nature*. 505:361-366.
10. Cafferkey M, Ahn JW, Flinter F, Ogilvie C (2014): Phenotypic features in patients with 15q11.2(BP1-BP2) deletion: further delineation of an emerging syndrome. *Am J Med Genet A*. 164A:1916-1922.
11. de Kovel CG, Trucks H, Helbig I, Mefford HC, Baker C, Leu C, et al. (2010): Recurrent microdeletions at 15q11.2 and 16p13.11 predispose to idiopathic generalized epilepsies. *Brain*. 133:23-32.

12. Ghani M, Pinto D, Lee JH, Grinberg Y, Sato C, Moreno D, et al. (2012): Genome-wide survey of large rare copy number variants in Alzheimer's disease among Caribbean hispanics. *G3 (Bethesda)*. 2:71-78.
13. Baldwin I, Shafer RL, Hossain WA, Gunewardena S, Veatch OJ, Mosconi MW, et al. (2021): Genomic, Clinical, and Behavioral Characterization of 15q11.2 BP1-BP2 Deletion (Burnside-Butler) Syndrome in Five Families. *Int J Mol Sci*. 22:1660.
14. Rafi SK, Butler MG (2020): The 15q11.2 BP1-BP2 Microdeletion (Burnside-Butler) Syndrome: In Silico Analyses of the Four Coding Genes Reveal Functional Associations with Neurodevelopmental Phenotypes. *Int J Mol Sci*. 21:3296.
15. Woo YJ, Kanellopoulos AK, Hemati P, Kirschen J, Nebel RA, Wang T, et al. (2019): Domain-Specific Cognitive Impairments in Humans and Flies With Reduced CYFIP1 Dosage. *Biol Psychiatry*. 86:306-314.
16. Silva AI, Kirov G, Kendall KM, Bracher-Smith M, Wilkinson LS, Hall J, et al. (2021): Analysis of Diffusion Tensor Imaging Data From the UK Biobank Confirms Dosage Effect of 15q11.2 Copy Number Variation on White Matter and Shows Association With Cognition. *Biol Psychiatry*. 90:307-316.
17. Writing Committee for the E-CNVWG, van der Meer D, Sonderby IE, Kaufmann T, Walters GB, Abdellaoui A, et al. (2020): Association of Copy Number Variation of the 15q11.2 BP1-BP2 Region With Cortical and Subcortical Morphology and Cognition. *JAMA Psychiatry*. 77:420-430.
18. De Rubeis S, Pasciuto E, Li KW, Fernandez E, Di Marino D, Buzzi A, et al. (2013): CYFIP1 coordinates mRNA translation and cytoskeleton remodeling to ensure proper dendritic spine formation. *Neuron*. 79:1169-1182.
19. Pathania M, Davenport EC, Muir J, Sheehan DF, Lopez-Domenech G, Kittler JT (2014): The autism and schizophrenia associated gene CYFIP1 is critical for the maintenance of dendritic complexity and the stabilization of mature spines. *Transl Psychiatry*. 4:e374.
20. Zhao L, Wang D, Wang Q, Rodal AA, Zhang YQ (2013): Drosophila cyfip regulates synaptic development and endocytosis by suppressing filamentous actin assembly. *PLoS Genet*. 9:e1003450.
21. Dominguez-Iturza N, Lo AC, Shah D, Armendariz M, Vannelli A, Mercaldo V, et al. (2019): The autism- and schizophrenia-associated protein CYFIP1 regulates bilateral brain connectivity and behaviour. *Nat Commun*. 10:3454.
22. Silva AI, Haddon JE, Ahmed Syed Y, Trent S, Lin TE, Patel Y, et al. (2019): Cyfip1 haploinsufficient rats show white matter changes, myelin thinning, abnormal oligodendrocytes and behavioural inflexibility. *Nat Commun*. 10:3455.

23. Kanellopoulos AK, Mariano V, Spinazzi M, Woo YJ, McLean C, Pech U, et al. (2020): Aralar Sequesters GABA into Hyperactive Mitochondria, Causing Social Behavior Deficits. *Cell*. 180:1178-1197 e1120.
24. Davenport EC, Szulc BR, Drew J, Taylor J, Morgan T, Higgs NF, et al. (2019): Autism and Schizophrenia-Associated CYFIP1 Regulates the Balance of Synaptic Excitation and Inhibition. *Cell Rep*. 26:2037-2051 e2036.
25. Stefansson H, Rujescu D, Cichon S, Pietilainen OP, Ingason A, Steinberg S, et al. (2008): Large recurrent microdeletions associated with schizophrenia. *Nature*. 455:232-236.
26. Mullen SA, Carvill GL, Bellows S, Bayly MA, Trucks H, Lal D, et al. (2013): Copy number variants are frequent in genetic generalized epilepsy with intellectual disability. *Neurology*. 81:1507-1514.
27. Nebel RA, Zhao D, Pedrosa E, Kirschen J, Lachman HM, Zheng D, et al. (2016): Reduced CYFIP1 in Human Neural Progenitors Results in Dysregulation of Schizophrenia and Epilepsy Gene Networks. *PLoS One*. 11:e0148039.
28. Peng J, Wang Y, He F, Chen C, Wu LW, Yang LF, et al. (2018): Novel West syndrome candidate genes in a Chinese cohort. *CNS Neurosci Ther*. 24:1196-1206.
29. De Rubeis S, He X, Goldberg AP, Poultney CS, Samocha K, Cicek AE, et al. (2014): Synaptic, transcriptional and chromatin genes disrupted in autism. *Nature*. 515:209-215.
30. Purcell SM, Moran JL, Fromer M, Ruderfer D, Solovieff N, Roussos P, et al. (2014): A polygenic burden of rare disruptive mutations in schizophrenia. *Nature*. 506:185-190.
31. Tam GW, van de Lagemaat LN, Redon R, Strathdee KE, Croning MD, Malloy MP, et al. (2010): Confirmed rare copy number variants implicate novel genes in schizophrenia. *Biochem Soc Trans*. 38:445-451.
32. Glessner JT, Wang K, Cai G, Korvatska O, Kim CE, Wood S, et al. (2009): Autism genome-wide copy number variation reveals ubiquitin and neuronal genes. *Nature*. 459:569-573.
33. Oguro-Ando A, Rosensweig C, Herman E, Nishimura Y, Werling D, Bill BR, et al. (2015): Increased CYFIP1 dosage alters cellular and dendritic morphology and dysregulates mTOR. *Mol Psychiatry*. 20:1069-1078.
34. Griesi-Oliveira K, Suzuki AM, Alves AY, Mafra A, Yamamoto GL, Ezquina S, et al. (2018): Actin cytoskeleton dynamics in stem cells from autistic individuals. *Sci Rep*. 8:11138.
35. Waltes R, Duketis E, Knapp M, Anney RJ, Huguet G, Schlitt S, et al. (2014): Common variants in genes of the postsynaptic FMRP signalling pathway are risk factors for autism spectrum disorders. *Hum Genet*. 133:781-792.

36. Toma C, Torrico B, Hervas A, Valdes-Mas R, Tristan-Noguero A, Padillo V, et al. (2014): Exome sequencing in multiplex autism families suggests a major role for heterozygous truncating mutations. *Mol Psychiatry*. 19:784-790.
37. Homsy J, Zaidi S, Shen Y, Ware JS, Samocha KE, Karczewski KJ, et al. (2015): De novo mutations in congenital heart disease with neurodevelopmental and other congenital anomalies. *Science*. 350:1262-1266.
38. Yuen RKC, Merico D, Bookman M, Howe LJ, Thiruvahindrapuram B, Patel RV, et al. (2017): Whole genome sequencing resource identifies 18 new candidate genes for autism spectrum disorder. *Nat Neurosci*. 20:602-611.
39. Yuen RK, Merico D, Cao H, Pellecchia G, Alipanahi B, Thiruvahindrapuram B, et al. (2016): Genome-wide characteristics of de novo mutations in autism. *NPJ Genom Med*. 1:160271-1602710.
40. Werling DM, Brand H, An JY, Stone MR, Zhu L, Glessner JT, et al. (2018): An analytical framework for whole-genome sequence association studies and its implications for autism spectrum disorder. *Nat Genet*. 50:727-736.
41. Turner TN, Coe BP, Dickel DE, Hoekzema K, Nelson BJ, Zody MC, et al. (2017): Genomic Patterns of De Novo Mutation in Simplex Autism. *Cell*. 171:710-722 e712.
42. Watanabe K, Stringer S, Frei O, Umicevic Mirkov M, de Leeuw C, Polderman TJC, et al. (2019): A global overview of pleiotropy and genetic architecture in complex traits. *Nat Genet*. 51:1339-1348.
43. Napoli I, Mercaldo V, Boyl PP, Eleuteri B, Zalfa F, De Rubeis S, et al. (2008): The fragile X syndrome protein represses activity-dependent translation through CYFIP1, a new 4E-BP. *Cell*. 134:1042-1054.
44. Takenawa T, Suetsugu S (2007): The WASP-WAVE protein network: connecting the membrane to the cytoskeleton. *Nat Rev Mol Cell Biol*. 8:37-48.
45. Chen Z, Borek D, Padrick SB, Gomez TS, Metlagel Z, Ismail AM, et al. (2010): Structure and control of the actin regulatory WAVE complex. *Nature*. 468:533-538.
46. Ding B, Yang S, Schaks M, Liu Y, Brown AJ, Rottner K, et al. (2022): Structures reveal a key mechanism of WAVE regulatory complex activation by Rac1 GTPase. *Nat Commun*. 13:5444.
47. Eden S, Rohatgi R, Podtelejnikov AV, Mann M, Kirschner MW (2002): Mechanism of regulation of WAVE1-induced actin nucleation by Rac1 and Nck. *Nature*. 418:790-793.
48. Kobayashi K, Kuroda S, Fukata M, Nakamura T, Nagase T, Nomura N, et al. (1998): p140Sra-1 (specifically Rac1-associated protein) is a novel specific target for Rac1 small GTPase. *J Biol Chem*. 273:291-295.

49. Steffen A, Rottner K, Ehinger J, Innocenti M, Scita G, Wehland J, et al. (2004): Sra-1 and Nap1 link Rac to actin assembly driving lamellipodia formation. *EMBO J*. 23:749-759.
50. Rottner K, Stradal TEB, Chen B (2021): WAVE regulatory complex. *Curr Biol*. 31:R512-R517.
51. Schaks M, Singh SP, Kage F, Thomason P, Klunemann T, Steffen A, et al. (2018): Distinct Interaction Sites of Rac GTPase with WAVE Regulatory Complex Have Non-redundant Functions in Vivo. *Curr Biol*. 28:3674-3684 e3676.
52. Stradal TE, Rottner K, Disanza A, Confalonieri S, Innocenti M, Scita G (2004): Regulation of actin dynamics by WASP and WAVE family proteins. *Trends Cell Biol*. 14:303-311.
53. Yang S, Tang Y, Liu Y, Brown AJ, Schaks M, Ding B, et al. (2022): Arf GTPase activates the WAVE regulatory complex through a distinct binding site. *Sci Adv*. 8:eadd1412.
54. Tada T, Sheng M (2006): Molecular mechanisms of dendritic spine morphogenesis. *Curr Opin Neurobiol*. 16:95-101.
55. Lewis TL, Jr., Courchet J, Polleux F (2013): Cell biology in neuroscience: Cellular and molecular mechanisms underlying axon formation, growth, and branching. *J Cell Biol*. 202:837-848.
56. Soderling SH, Guire ES, Kaech S, White J, Zhang F, Schutz K, et al. (2007): A WAVE-1 and WRP signaling complex regulates spine density, synaptic plasticity, and memory. *J Neurosci*. 27:355-365.
57. Spence EF, Soderling SH (2015): Actin Out: Regulation of the Synaptic Cytoskeleton. *J Biol Chem*. 290:28613-28622.
58. Jacquemont S, Pacini L, Jonch AE, Cencelli G, Rozenberg I, He Y, et al. (2018): Protein synthesis levels are increased in a subset of individuals with fragile X syndrome. *Hum Mol Genet*. 27:2039-2051.
59. Cencelli G, Pacini L, De Luca A, Messia I, Gentile A, Kang Y, et al. (2023): Age-Dependent Dysregulation of APP in Neuronal and Skin Cells from Fragile X Individuals. *Cells*. 12:758.
60. Riedl J, Crevenna AH, Kessenbrock K, Yu JH, Neukirchen D, Bista M, et al. (2008): Lifeact: a versatile marker to visualize F-actin. *Nat Methods*. 5:605-607.
61. Doggett TM, Breslin JW (2011): Study of the actin cytoskeleton in live endothelial cells expressing GFP-actin. *J Vis Exp*. 57:3187.
62. Mariano V, Kanellopoulos AK, Aiello G, Lo AC, Legius E, Achsel T, et al. (2023): SREBP modulates the NADP(+)/NADPH cycle to control night sleep in Drosophila. *Nat Commun*. 14:763.
63. Association AP (2013): DSM-5 Diagnostic Classification. *Diagnostic and Statistical Manual of Mental Disorders*, 5th edition, text rev. ed: American Psychiatric Association.

64. Chen B, Brinkmann K, Chen Z, Pak CW, Liao Y, Shi S, et al. (2014): The WAVE regulatory complex links diverse receptors to the actin cytoskeleton. *Cell*. 156:195-207.
65. Di Marino D, Chillemi G, De Rubeis S, Tramontano A, Achsel T, Bagni C (2015): MD and Docking Studies Reveal That the Functional Switch of CYFIP1 is Mediated by a Butterfly-like Motion. *J Chem Theory Comput*. 11:3401-3410.
66. Chen B, Chou HT, Brautigam CA, Xing W, Yang S, Henry L, et al. (2017): Rac1 GTPase activates the WAVE regulatory complex through two distinct binding sites. *Elife*. 6:e29795.
67. Kawano Y, Yoshimura T, Tsuboi D, Kawabata S, Kaneko-Kawano T, Shirataki H, et al. (2005): CRMP-2 is involved in kinesin-1-dependent transport of the Sra-1/WAVE1 complex and axon formation. *Mol Cell Biol*. 25:9920-9935.
68. Santini E, Huynh TN, Longo F, Koo SY, Mojica E, D'Andrea L, et al. (2017): Reducing eIF4E-eIF4G interactions restores the balance between protein synthesis and actin dynamics in fragile X syndrome model mice. *Sci Signal*. 10:eaan0665.
69. Parenti I, Rabaneda LG, Schoen H, Novarino G (2020): Neurodevelopmental Disorders: From Genetics to Functional Pathways. *Trends Neurosci*. 43:608-621.
70. Kelleher RJ, 3rd, Bear MF (2008): The autistic neuron: troubled translation? *Cell*. 135:401-406.
71. Mercaldo V, Vidimova B, Gastaldo D, Fernandez E, Lo AC, Cencelli G, et al. (2023): Altered striatal actin dynamics drives behavioral inflexibility in a mouse model of fragile X syndrome. *Neuron*. 111:1760-1775 e1768.
72. Gkogkas CG, Khoutorsky A, Ran I, Rampakakis E, Nevarko T, Weatherill DB, et al. (2013): Autism-related deficits via dysregulated eIF4E-dependent translational control. *Nature*. 493:371-377.
73. Wiebe S, Nagpal A, Sonenberg N (2020): Dysregulated translational control in brain disorders: from genes to behavior. *Curr Opin Genet Dev*. 65:34-41.
74. Longo F, Klann E (2021): Reciprocal control of translation and transcription in autism spectrum disorder. *EMBO Rep*. 22:e52110.
75. Schmidt EK, Clavarino G, Ceppi M, Pierre P (2009): SUnSET, a nonradioactive method to monitor protein synthesis. *Nat Methods*. 6:275-277.
76. Svitkina T (2018): The Actin Cytoskeleton and Actin-Based Motility. *Cold Spring Harb Perspect Biol*. 10:a018267.
77. Dupraz S, Hilton BJ, Husch A, Santos TE, Coles CH, Stern S, et al. (2019): RhoA Controls Axon Extension Independent of Specification in the Developing Brain. *Curr Biol*. 29:3874-3886 e3879.

78. Pollard TD, Borisy GG (2003): Cellular motility driven by assembly and disassembly of actin filaments. *Cell*. 112:453-465.
79. Suraneni P, Rubinstein B, Unruh JR, Durnin M, Hanein D, Li R (2012): The Arp2/3 complex is required for lamellipodia extension and directional fibroblast cell migration. *J Cell Biol*. 197:239-251.
80. van der Voet M, Nijhof B, Oortveld MA, Schenck A (2014): Drosophila models of early onset cognitive disorders and their clinical applications. *Neurosci Biobehav Rev*. 46 Pt 2:326-342.
81. Coll-Tane M, Krebbers A, Castells-Nobau A, Zweier C, Schenck A (2019): Intellectual disability and autism spectrum disorders 'on the fly': insights from Drosophila. *Dis Model Mech*. 12:dmm039180.
82. Mariano V, Achsel T, Bagni C, Kanellopoulos AK (2020): Modelling Learning and Memory in Drosophila to Understand Intellectual Disabilities. *Neuroscience*. 445:12-30.
83. Schenck A, Bardoni B, Langmann C, Harden N, Mandel JL, Giangrande A (2003): CYFIP/Sra-1 controls neuronal connectivity in Drosophila and links the Rac1 GTPase pathway to the fragile X protein. *Neuron*. 38:887-898.
84. Cioni JM, Wong HH, Bressan D, Kodama L, Harris WA, Holt CE (2018): Axon-Axon Interactions Regulate Topographic Optic Tract Sorting via CYFIP2-Dependent WAVE Complex Function. *Neuron*. 97:1078-1093 e1076.
85. Fernandez MP, Berni J, Ceriani MF (2008): Circadian remodeling of neuronal circuits involved in rhythmic behavior. *PLoS Biol*. 6:e69.
86. Kozlov SV, Bogenpohl JW, Howell MP, Wevrick R, Panda S, Hogenesch JB, et al. (2007): The imprinted gene Magel2 regulates normal circadian output. *Nat Genet*. 39:1266-1272.
87. Petsakou A, Sapsis TP, Blau J (2015): Circadian Rhythms in Rho1 Activity Regulate Neuronal Plasticity and Network Hierarchy. *Cell*. 162:823-835.
88. Zwarts L, Vanden Broeck L, Cappuyns E, Ayroles JF, Magwire MM, Vulsteke V, et al. (2015): The genetic basis of natural variation in mushroom body size in Drosophila melanogaster. *Nat Commun*. 6:10115.
89. Rollmann SM, Zwarts L, Edwards AC, Yamamoto A, Callaerts P, Norga K, et al. (2008): Pleiotropic effects of Drosophila neuralized on complex behaviors and brain structure. *Genetics*. 179:1327-1336.
90. Bachmann SO, Sledziowska M, Cross E, Kalbassi S, Waldron S, Chen F, et al. (2019): Behavioral training rescues motor deficits in Cyfip1 haploinsufficiency mouse model of autism spectrum disorders. *Transl Psychiatry*. 9:29.

91. Kim NS, Ringeling FR, Zhou Y, Nguyen HN, Temme SJ, Lin YT, et al. (2022): CYFIP1 Dosages Exhibit Divergent Behavioral Impact via Diametric Regulation of NMDA Receptor Complex Translation in Mouse Models of Psychiatric Disorders. *Biol Psychiatry*. 92:815-826.
92. Simon AF, Chou MT, Salazar ED, Nicholson T, Saini N, Metchev S, et al. (2012): A simple assay to study social behavior in Drosophila: measurement of social space within a group. *Genes Brain Behav*. 11:243-252.
93. Jiang L, Cheng Y, Gao S, Zhong Y, Ma C, Wang T, et al. (2020): Emergence of social cluster by collective pairwise encounters in Drosophila. *Elife*. 9:e51921.
94. Gargano JW, Martin I, Bhandari P, Grotewiel MS (2005): Rapid iterative negative geotaxis (RING): a new method for assessing age-related locomotor decline in Drosophila. *Exp Gerontol*. 40:386-395.
95. Hsiao K, Harony-Nicolas H, Buxbaum JD, Bozdagi-Gunal O, Benson DL (2016): Cyfip1 Regulates Presynaptic Activity during Development. *J Neurosci*. 36:1564-1576.
96. Di Marino D, D'Annessa I, Tancredi H, Bagni C, Gallicchio E (2015): A unique binding mode of the eukaryotic translation initiation factor 4E for guiding the design of novel peptide inhibitors. *Protein Sci*. 24:1370-1382.
97. Bieling P, Hansen SD, Akin O, Li TD, Hayden CC, Fletcher DA, et al. (2018): WH2 and proline-rich domains of WASP-family proteins collaborate to accelerate actin filament elongation. *EMBO J*. 37:102-121.
98. Pollard TD, Blanchoin L, Mullins RD (2000): Molecular mechanisms controlling actin filament dynamics in nonmuscle cells. *Annu Rev Biophys Biomol Struct*. 29:545-576.
99. Rotty JD, Wu C, Bear JE (2013): New insights into the regulation and cellular functions of the ARP2/3 complex. *Nat Rev Mol Cell Biol*. 14:7-12.
100. Adzhubei IA, Schmidt S, Peshkin L, Ramensky VE, Gerasimova A, Bork P, et al. (2010): A method and server for predicting damaging missense mutations. *Nat Methods*. 7:248-249.
101. Whitelaw JA, Swaminathan K, Kage F, Machesky LM (2020): The WAVE Regulatory Complex Is Required to Balance Protrusion and Adhesion in Migration. *Cells*. 9:1635.
102. Yamazaki D, Fujiwara T, Suetsugu S, Takenawa T (2005): A novel function of WAVE in lamellipodia: WAVE1 is required for stabilization of lamellipodial protrusions during cell spreading. *Genes Cells*. 10:381-392.
103. Sweeney MO, Collins A, Padrick SB, Goode BL (2015): A novel role for WAVE1 in controlling actin network growth rate and architecture. *Mol Biol Cell*. 26:495-505.
104. Suetsugu S, Yamazaki D, Kurisu S, Takenawa T (2003): Differential roles of WAVE1 and WAVE2 in dorsal and peripheral ruffle formation for fibroblast cell migration. *Dev Cell*. 5:595-609.

105. Tahirovic S, Hellal F, Neukirchen D, Hindges R, Garvalov BK, Flynn KC, et al. (2010): Rac1 regulates neuronal polarization through the WAVE complex. *J Neurosci*. 30:6930-6943.
106. Begemann A, Sticht H, Begtrup A, Vitobello A, Faivre L, Banka S, et al. (2021): New insights into the clinical and molecular spectrum of the novel CYFIP2-related neurodevelopmental disorder and impairment of the WRC-mediated actin dynamics. *Genet Med*. 23:543-554.
107. Yan Z, Kim E, Datta D, Lewis DA, Soderling SH (2016): Synaptic Actin Dysregulation, a Convergent Mechanism of Mental Disorders? *J Neurosci*. 36:11411-11417.
108. Parviainen L, Dihanich S, Anderson GW, Wong AM, Brooks HR, Abeti R, et al. (2017): Glial cells are functionally impaired in juvenile neuronal ceroid lipofuscinosis and detrimental to neurons. *Acta Neuropathol Commun*. 5:74.
109. Thomason EJ, Escalante M, Osterhout DJ, Fuss B (2020): The oligodendrocyte growth cone and its actin cytoskeleton: A fundamental element for progenitor cell migration and CNS myelination. *Glia*. 68:1329-1346.
110. Rubenstein JL, Merzenich MM (2003): Model of autism: increased ratio of excitation/inhibition in key neural systems. *Genes Brain Behav*. 2:255-267.
111. Nakashima M, Kato M, Aoto K, Shiina M, Belal H, Mukaida S, et al. (2018): De novo hotspot variants in CYFIP2 cause early-onset epileptic encephalopathy. *Ann Neurol*. 83:794-806.
112. Zweier M, Begemann A, McWalter K, Cho MT, Abela L, Banka S, et al. (2019): Spatially clustering de novo variants in CYFIP2, encoding the cytoplasmic FMRP interacting protein 2, cause intellectual disability and seizures. *Eur J Hum Genet*. 27:747-759.
113. Spillane M, Gallo G (2014): Involvement of Rho-family GTPases in axon branching. *Small GTPases*. 5:e27974.
114. Bradke F (2022): Mechanisms of Axon Growth and Regeneration: Moving between Development and Disease. *J Neurosci*. 42:8393-8405.
115. MacDonald M, Lord C, Ulrich D (2013): The relationship of motor skills and adaptive behavior skills in young children with autism spectrum disorders. *Res Autism Spectr Disord*. 7:1383-1390.
116. Doan RN, Lim ET, De Rubeis S, Betancur C, Cutler DJ, Chiocchetti AG, et al. (2019): Recessive gene disruptions in autism spectrum disorder. *Nat Genet*. 51:1092-1098.
117. Bacchelli E, Ceroni F, Pinto D, Lomartire S, Giannandrea M, D'Adamo P, et al. (2014): A CTNNA3 compound heterozygous deletion implicates a role for alphaT-catenin in susceptibility to autism spectrum disorder. *J Neurodev Disord*. 6:17.

118. Siu WK, Lam CW, Gao WW, Vincent Tang HM, Jin DY, Mak CM (2016): Unmasking a novel disease gene NEO1 associated with autism spectrum disorders by a hemizygous deletion on chromosome 15 and a functional polymorphism. *Behav Brain Res*. 300:135-142.

119. Vorstman JA, van Daalen E, Jalali GR, Schmidt ER, Pasterkamp RJ, de Jonge M, et al. (2011): A double hit implicates DIAPH3 as an autism risk gene. *Mol Psychiatry*. 16:442-451.

120. Lim ET, Raychaudhuri S, Sanders SJ, Stevens C, Sabo A, MacArthur DG, et al. (2013): Rare complete knockouts in humans: population distribution and significant role in autism spectrum disorders. *Neuron*. 77:235-242.

121. Schenck A, Bardoni B, Moro A, Bagni C, Mandel JL (2001): A highly conserved protein family interacting with the fragile X mental retardation protein (FMRP) and displaying selective interactions with FMRP-related proteins FXR1P and FXR2P. *Proc Natl Acad Sci U S A*. 98:8844-8849.

KEY RESOURCES TABLE

Resource Type	Specific Reagent or Resource	Source or Reference	Identifiers	Additional Information
Add additional rows as needed for each resource type	Include species and sex when applicable.	Include name of manufacturer, company, repository, individual, or research lab. Include PMID or DOI for references; use “this paper” if new.	Include catalog numbers, stock numbers, database IDs or accession numbers, and/or RRIDs. RRIDs are highly encouraged; search for RRIDs at https://scicrunch.org/resources.	Include any additional information or notes if necessary.

Table 1. Clinical features of individuals with recessive *CYFIP1* missense variants.

	Individual 1 (II-2) – Proband 1	**Individual 2 (II-3)**
***CYFIP1* variant**	p.(Ile476Val); p.(Pro746Val)	p.(Ile476Val); p.(Pro746Val)
Inheritance	p.(Ile476Val) paternal p.(Pro746Val) maternal	p.(Ile476Val) paternal p.(Pro746Val) maternal
Sex	Male	Male
Gestational age (weeks)	39 (amenorrhea)	40 (amenorrhea)
Birth HC/length/weight standard deviations	32,5cm (-2 SD) /50 cm (M)/3315gr (M)	32 cm (–2 SD)/ 48 (-1,5 SD)/ 2630gr (-1,5 SD)
HC/length/weight at last investigation standard deviations	52 cm (-3SD)/ 157 cm (-3SD)/ 43,5 Kgs (-2,5SD) at 17,5 years	48 cm (-3SD)/ 120,5 cm (M)/ 23,4kgs (-1SD) at 9 years
Microcephaly	Yes	Yes
Morphological features	Large mouth, thick lips, hypertelorism, low hairline	Large mouth, thick lips, hypertelorism, low hairline
Developmental delay	Severe developmental delay can sit up, walk with assistance	Severe developmental delay can sit up, walk with assistance
Age at unassisted sitting	4 years	1 year
Age at independent walking	No independent walking	No independent walking
Age at first words	No words	No words
Age at last evaluation	17 years and 8 months old	13 years et 4 months old
Speech development	Non-verbal	Non-verbal
Intellectual disability	Profound	Profound
Abnormal behavior	Paroxysmal bursts of laughter/ pseudo-Angelman behavior (happy demeanor) Hyperactivity Repetitive behavior (head banging)	Unmotivated laughter/ pseudo-Angelm behavior (happy demeanor)
Seizure (age of onset)	Yes (3 years)	Yes (6 years)
Epilepsy syndrome	Yes	Yes
Seizure type/ medicament	Absence seizures / ZONISAMIDE and valproate	Absence seizures / valproate
Current seizure frequency	Several times a week	Stabilized epilepsy
EEG findings	Paroxysm	Slow track
Cerebral MRI findings	FLAIR hyper signal in the thalamus, moderate ventriculomegaly, normal spectroscopy	Normal
Muscular hypo-/hypertonia	Spasticity of the lower limbs, pyramidal syndrome	Trunk ataxia
Other neurological issues	Autistic symptoms	Autistic symptoms
Other features	Scoliosis (arthrodesis), strabismus	Valgus flat feet (arthrodesis)

Abbreviations: HC: head circumference; EEG: electroencephalogram; MRI: magnetic resonance imaging.

Table 2. Detection of the SNVs by Sanger sequencing in the proband 1 and prediction of pathogenicity.

Gene variant	Genomic position	Mode of transmission	Dbsnp	PolyPhen-2	SIFT	CADD phred	Revel	GnomAD v3	SPiP prediction	Reason for exclusion
CLCN3 (c.2031G>A p.Val677=)	chr4:g.170628299G>A	*De novo*	Not reported	Benign	Tolerated			Not reported		Considered benign by all predicting bioinformatic softwares; Not present in proband 2
SFI1 (c.1323G>A p.Leu441=)	chr22:g.31985435G>A	*De novo*	rs1479552764	Benign	Benign			Not reported		Considered benign by all predicting bioinformatic softwares; Not present in proband 2
POLA1 (c.617C>T p.Thr206Met)	chrX:g.24734570C>T	X-linked	rs200356660	Benign	Tolerated	7.66	Benign	5/112242	69.33% risk of altering the consensus splice site	Considered benign/tolerated by SIFT, CADD, PolyPhen2, REVEL; Not present in proband 2
MAGEB2 (c.47G>A p.Arg16His)	chrX:g.30236744G>A	X-linked	rs151181148	Possibly damaging	Tolerated	10.29	Benign	33/112089		Considered benign/tolerated by SIFT, CADD, REVEL; Not present in proband 2
SMC1A (c.861G>A p.Lys287=)	chrX:g.53439197C>T	X-linked	rs782543093	Benign	Benign			13/111573		Considered benign by all predicting bioinformatic softwares;
UXT (c.264C>G p.Asn88Lys)	chrX:g.47516991G>C	X-linked	Not reported	Probably damaging	Damaging	24.1	Uncertain	Not reported	30.67% risk of creation of a new splice site	Gene involved in syndromic disorder that cannot explain the probands phenotype (124)
IFIH1 (c.1230T>G p.Ile410Met)	chr2:g.163138952A>C	Recessive	Not reported	Probably damaging	Damaging	22.70		Not reported		Inherited from the unaffected father; Not present in proband 2
IFIH1 (c.949C>T p.Gln317*)	chr2:g.163144791G>A	Recessive	rs74162079			37.00		5/151872		Inherited from the unaffected mother; Loss of function of the gene is related to syndromic disorders that cannot explain the probands phenotype (125)

TTN (c.89846C>T p.Thr29949Ile)	chr2:g.179417781G>A	recessive	rs1284316750	Possibly damaging	Damaging	22.5	Uncertain	1/247238		Not present in proband 2
TTN (c.55378A>G p.Thr18460Ala)	chr2:g.179466439T>C	recessive	rs727503600	Probably damaging	Tolerated	24.00	Uncertain	17/152066		Gene involved in syndromic disorder that cannot explain the probands phenotype (126)
CYFIP1 (c.1426A>G p.Ile476Val)	chr15:g.22954276A>G	recessive	rs148341871	Possibly damaging	Tolerated	22.70	Benign	15/152142		//
CYFIP1 (c.2225C>T p.Pro742Leu)	chr15:g.22962505C>T	recessive	rs139576657	Benign	Tolerated	23.40	Benign	6/152210		//
SCAF1 (c.436A>C p.S146R)	chr19:g.50150045A>C	recessive	Not reported	Benign	Damaging	23.8	Benign	Not reported		Not present in proband 2
SCAF1 (c.3181G>A p.A1061T	chr19:g.50156827G>A	recessive	rs183980772	Benign	Damaging	22.8	Benign	42/152020		Not present in proband 2

Selected variants have been narrowed down using consecutive filters based on different models of inheritance (*De novo*, X-linked and recessive) and damage prediction scores (PolyPhen-2 (102), SIFT (127), CADD (128), Revel (129) and SPiP (130)). All the variants listed have been checked for their presence in the second affected individual (II-3).

Figure 1.

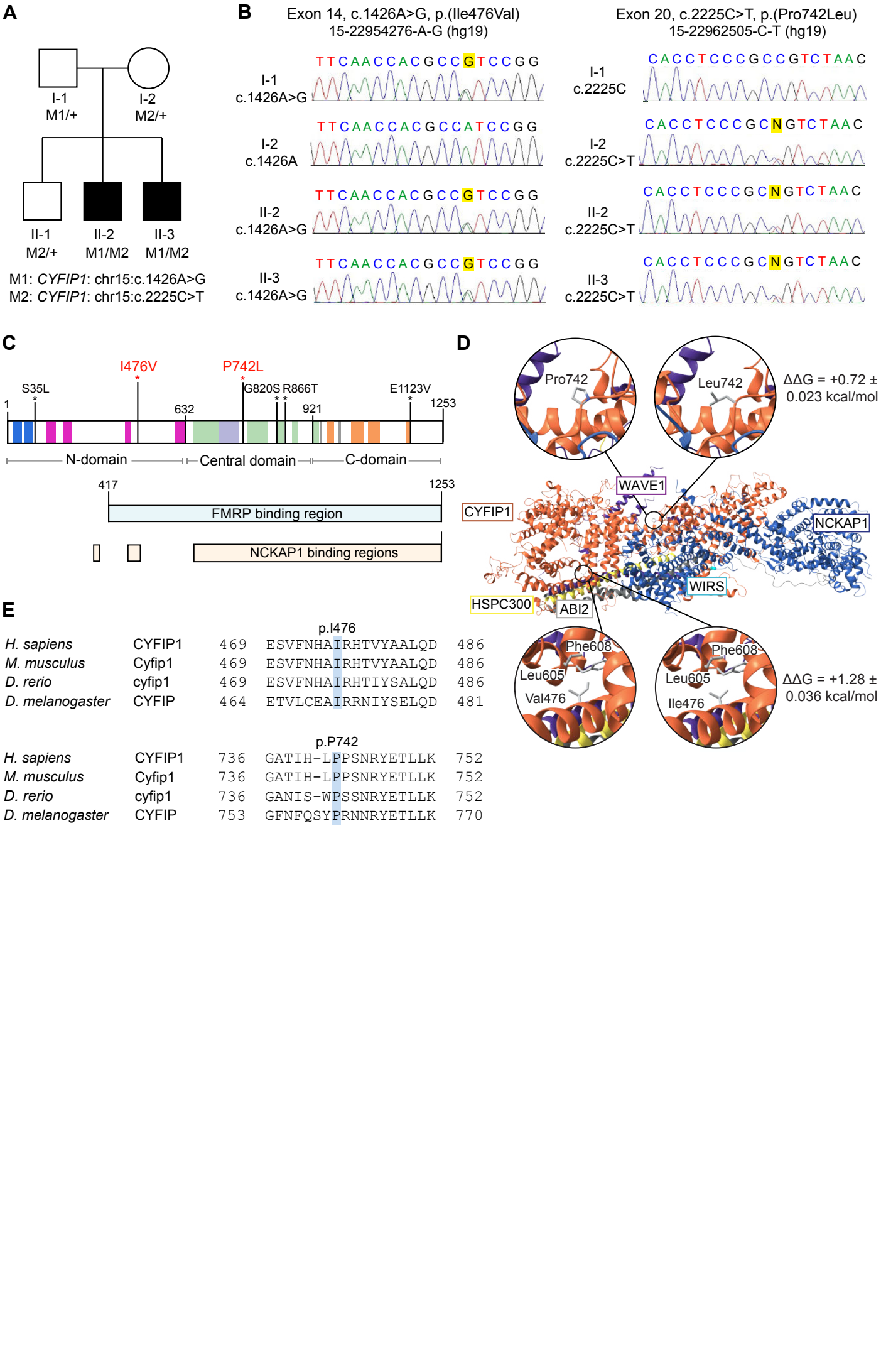
A
I-1
M1/+
I-2
M2/+
II-1
M2/+
II-2
M1/M2
II-3
M1/M2
M1: CYFIP1: chr15:c.1426A>G
M2: CYFIP1: chr15:c.2225C>T
B
Exon 14, c.1426A>G, p.(Ile476Val)
15-22954276-A-G (hg19)
Exon 20, c.2225C>T, p.(Pro742Leu)
15-22962505-C-T (hg19)
I-1
c.1426A>G
I-2
c.1426A
II-2
c.1426A>G
II-3
c.1426A>G
I-1
c.2225C
I-2
c.2225C>T
II-2
c.2225C>T
II-3
c.2225C>T
C
I476V
P742L
S35L
G820S
R866T
E1123V
1
632
921
1253
N-domain
Central domain
C-domain
417
1253
FMRP binding region
NCKAP1 binding regions
D
Pro742
Leu742
ΔΔG = +0.72 ± 0.023 kcal/mol
WAVE1
CYFIP1
NCKAP1
WIRS
HSPC300
ABI2
Phe608
Leu605
Val476
Phe608
Leu605
Ile476
ΔΔG = +1.28 ± 0.036 kcal/mol
E
p.I476
H. sapiens CYFIP1 469 ESVFNHAIRHTVYAALQD 486
M. musculus Cyfip1 469 ESVFNHAIRHTVYAALQD 486
D. rerio cyfip1 469 ESVFNHAIRHTIYSALQD 486
D. melanogaster CYFIP 464 ETVLCEAIRRNIYSELQD 481
p.P742
H. sapiens CYFIP1 736 GATIH-LPPSNRYETLLK 752
M. musculus Cyfip1 736 GATIH-LPPSNRYETLLK 752
D. rerio cyfip1 736 GANIS-WPSSNRYETLLK 752
D. melanogaster CYFIP 753 GFNFQSYPRNNRYETLLK 770

Figure 2.

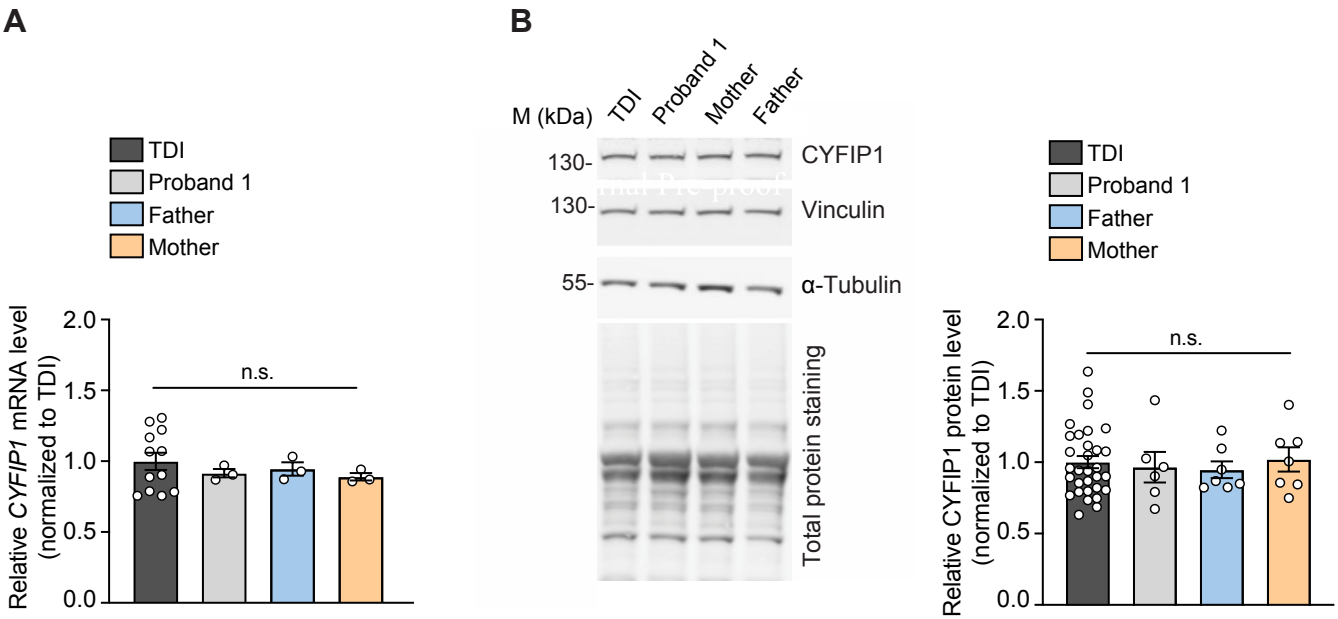
A
TDI
Proband 1
Father
Mother
Relative CYFIP1 mRNA level (normalized to TDI)
2.0
1.5
1.0
0.5
0.0
n.s.
B
M (kDa)
TDI
Proband 1
Mother
Father
130-
CYFIP1
130-
Vinculin
55-
α-Tubulin
Total protein staining
TDI
Proband 1
Father
Mother
Relative CYFIP1 protein level (normalized to TDI)
2.0
1.5
1.0
0.5
0.0
n.s.

Figure 3.

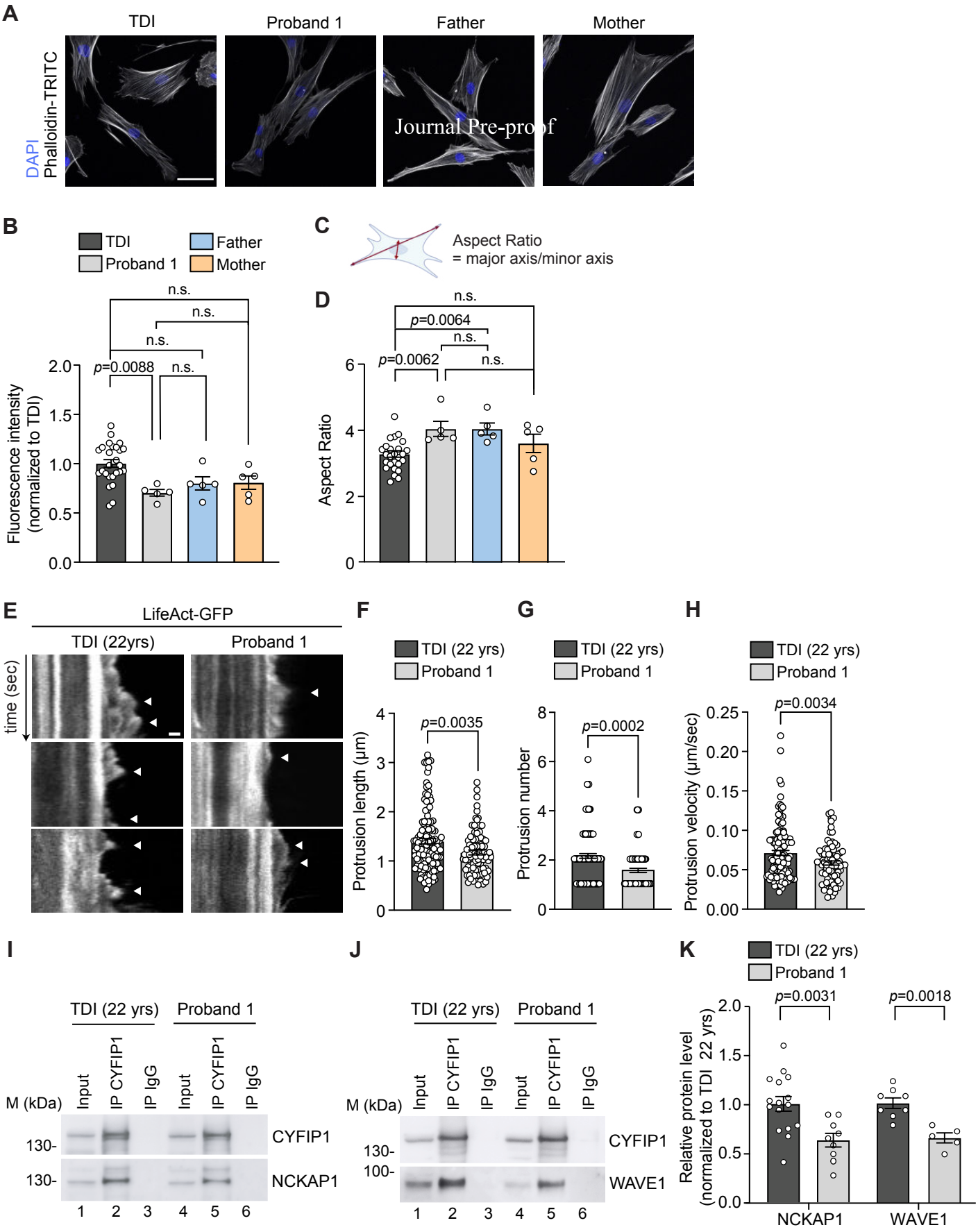
A
TDI
Proband 1
Father
Mother
DAPI
Phalloidin-TRITC
Journal Pre-proof
B
TDI
Proband 1
Father
Mother
n.s.
n.s.
n.s.
p=0.0088
n.s.
Fluorescence intensity (normalized to TDI)
C
Aspect Ratio
= major axis/minor axis
D
n.s.
p=0.0064
n.s.
p=0.0062
n.s.
Aspect Ratio
E
LifeAct-GFP
TDI (22yrs)
Proband 1
time (sec)
F
TDI (22 yrs)
Proband 1
p=0.0035
Protrusion length (μm)
G
TDI (22 yrs)
Proband 1
p=0.0002
Protrusion number
H
TDI (22 yrs)
Proband 1
p=0.0034
Protrusion velocity (μm/sec)
I
TDI (22 yrs)
Proband 1
Input
IP CYFIP1
IP IgG
M (kDa)
130-
CYFIP1
NCKAP1
1 2 3 4 5 6
J
TDI (22 yrs)
Proband 1
Input
IP CYFIP1
IP IgG
M (kDa)
130-
100-
CYFIP1
WAVE1
1 2 3 4 5 6
K
TDI (22 yrs)
Proband 1
p=0.0031
p=0.0018
Relative protein level (normalized to TDI 22 yrs)
NCKAP1
WAVE1

Figure 4.

A

Aligment			Identity	Similarity	DIOPT
CYFIP1 Human	469 ESVFNHA**I**RHTVYAALQD	p.I476V	65%	80%	15/18
CYFIP *Drosophila*	464 ETVLCEA**I**RRNIYSELQD	p.I471V			
CYFIP1 Human	736 GATIH-L**P**PSNRYETLLK	p.P742L			
CYFIP *Drosophila*	753 GFNFQSY**P**RNNRYETLLK	p.P760L			

B

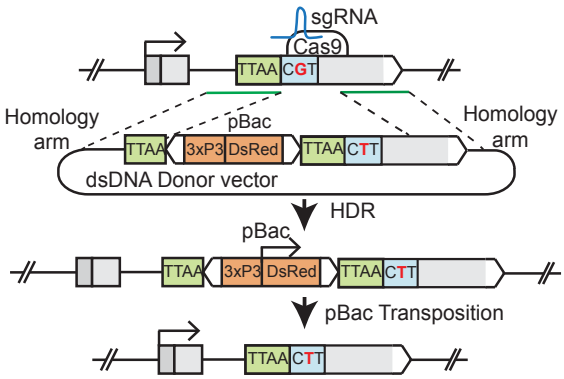

Cyfip^{I471V}	Homozygous viable
Cyfip^{P760L}	Homozygous viable

C

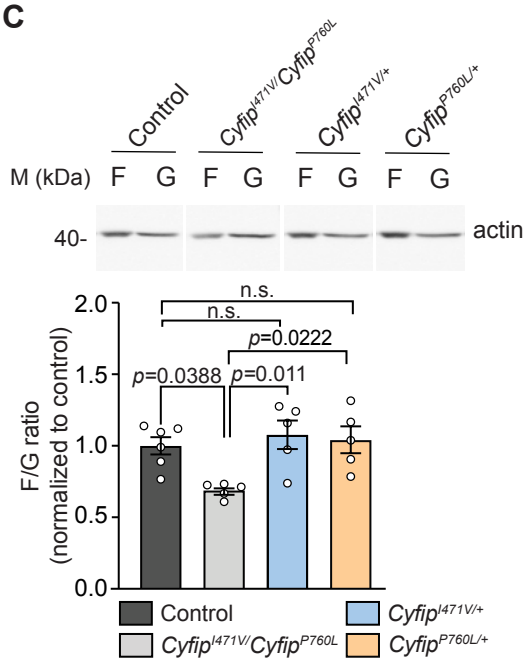

D

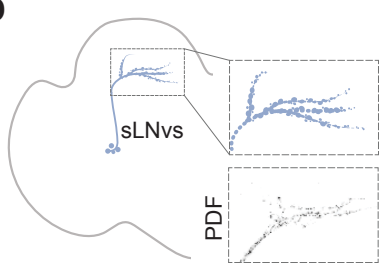

E

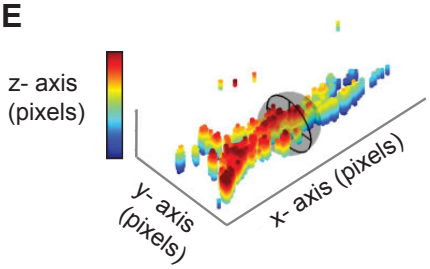

F

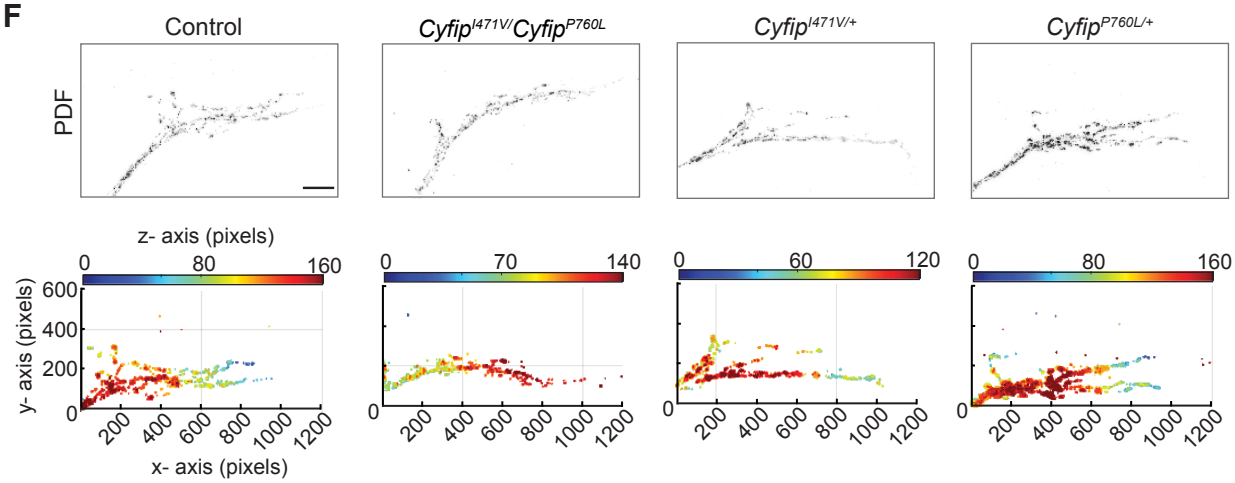

G

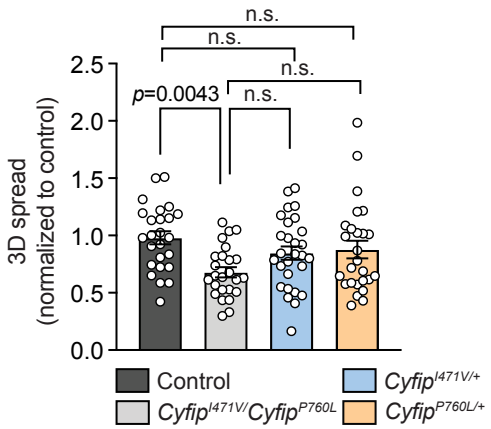

H

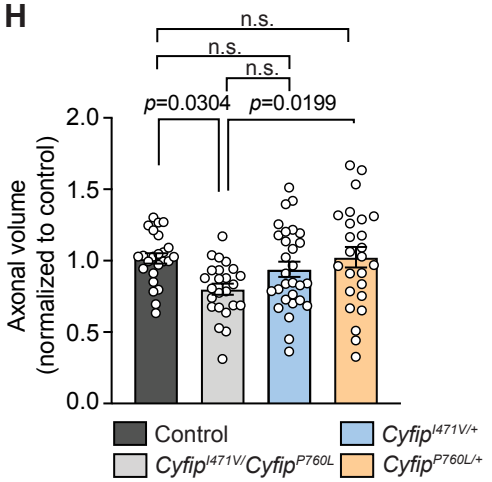

Figure 5.

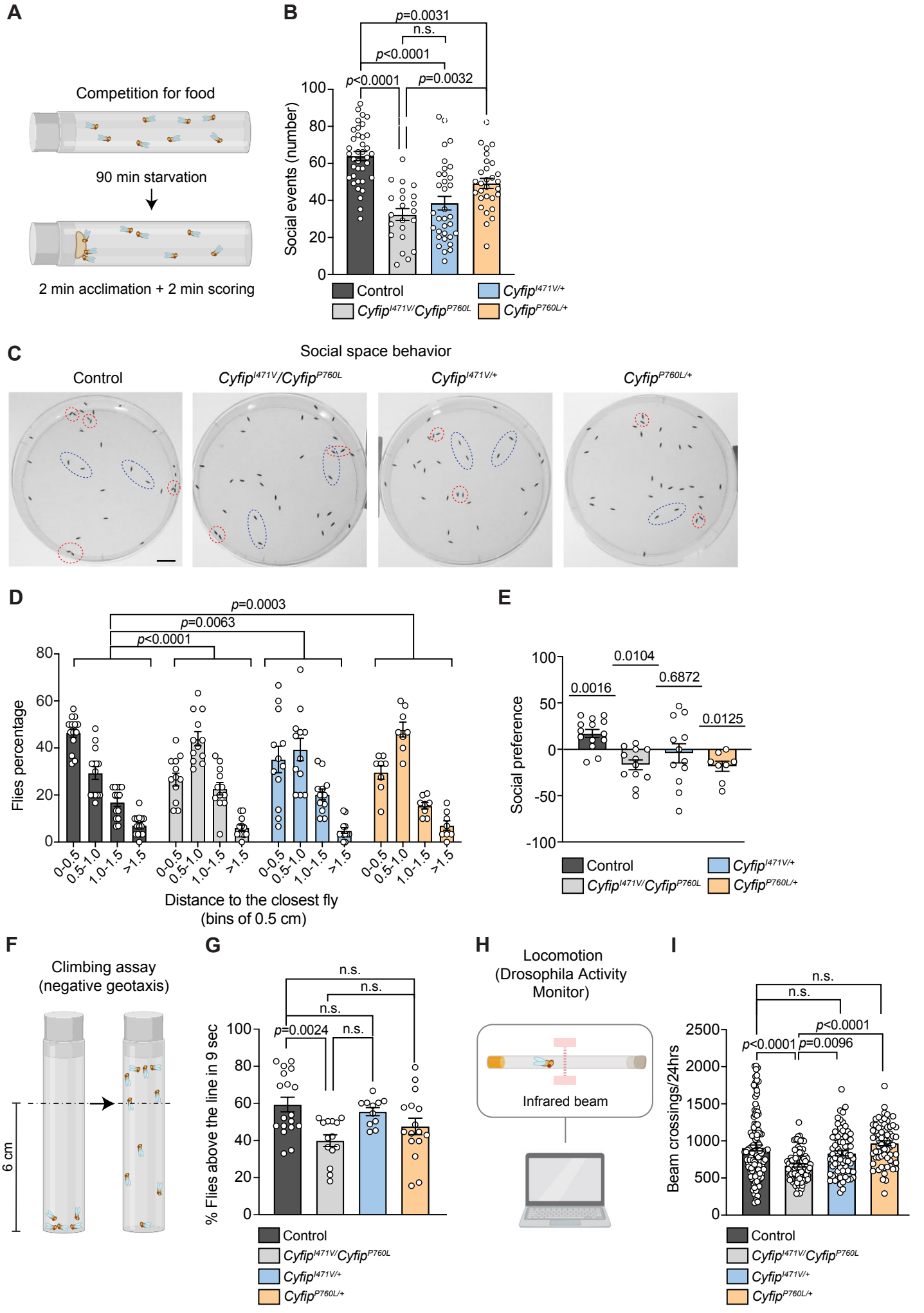
A
Competition for food
90 min starvation
2 min acclimation + 2 min scoring
B
p=0.0031
n.s.
p<0.0001
p<0.0001
p=0.0032
Social events (number)
Control
Cyfip I471V/+
Cyfip I471V/Cyfip P760L
Cyfip P760L/+
C
Social space behavior
Control
Cyfip I471V/Cyfip P760L
Cyfip I471V/+
Cyfip P760L/+
D
p=0.0003
p=0.0063
p<0.0001
Flies percentage
0-0.5
0.5-1.0
1.0-1.5
>1.5
Distance to the closest fly
(bins of 0.5 cm)
E
0.0104
0.0016
0.6872
0.0125
Social preference
Control
Cyfip I471V/+
Cyfip I471V/Cyfip P760L
Cyfip P760L/+
F
Climbing assay
(negative geotaxis)
6 cm
G
n.s.
n.s.
n.s.
p=0.0024
n.s.
% Flies above the line in 9 sec
Control
Cyfip I471V/Cyfip P760L
Cyfip I471V/+
Cyfip P760L/+
H
Locomotion
(Drosophila Activity
Monitor)
Infrared beam
I
n.s.
n.s.
p<0.0001
p<0.0001
p=0.0096
Beam crossings/24hrs
Control
Cyfip I471V/Cyfip P760L
Cyfip I471V/+
Cyfip P760L/+